Axicon Lens for Electrons Using a Magnetic Vortex: The Efficient Generation of a Bessel Beam

Changlin Zheng,[1] Timothy C. Petersen,[2] Holm Kirmse,[3] Wolfgang Neumann,[3,4] Michael J. Morgan,[2] and Joanne Etheridge[1,5,*]

[1]*Monash Centre for Electron Microscopy, Monash University, Victoria 3800, Australia*
[2]*School of Physics and Astronomy, Monash University, Victoria 3800, Australia*
[3]*Institute of Physics, Humboldt University of Berlin, D-12489 Berlin, Germany*
[4]*Department of Chemistry and Biochemistry, University of Oregon, Eugene, Oregon 97403, USA*
[5]*Department of Materials Science and Engineering, Monash University, Victoria 3800, Australia*

(Received 23 February 2017; published 25 October 2017)

We demonstrate experimentally an efficient electron axicon lens using a magnetic vortex. We show that naturally occurring magnetic vortices with circular magnetic moment distributions in a soft-magnetic thin film create conical phase shifts for fast electrons. Such radially symmetric linear phase ramps are equivalent to ideal light optical axicons. We apply this lens to generate efficient nondiffracting electron Bessel beams, which we observe experimentally in through-focus Lorentz images as well as in propagated off-axis electron holograms. This highlights the potential for using magnetic nanostructures as highly efficient and flexible phase plates for crafting desired electron beam shapes.

DOI: 10.1103/PhysRevLett.119.174801

Modern transmission electron microscopy (TEM) has embraced the physics of singular and nondiffracting optics to generate a variety of interesting new electron probes, including so-called electron vortex beams [1–8], Airy beams [9,10], and Bessel beams [11,12]. These enable new diffraction physics and electron-matter interactions that are intrinsically interesting [1–7,13] and promise significant practical uses, including the manipulation of nanoparticles [14], the detection of surface plasmon polariton symmetries [15], and the characterization of Landau states [16] and chiral specimens [17]. Furthermore, electron Bessel beams can enable the measurement of valence electron energy loss spectra with a spatial resolution exceeding that limited by delocalization [18], can be spin polarized in an electron microscope [19], and have potential for use in electron tomography where a large depth of focus [20] improves imaging for tilted fields of view [11].

"Bessel beams" arise from the Helmholtz equation, which admits solutions that are invariant with respect to free space propagation [21], known as nondiffracting beams [22]. Perhaps the simplest beamlike solution is a scalar wave function, where the amplitude takes the form of a Bessel function of the first kind and is independent of the propagation distance. Thus, the intensity of the beam, in particular, the central maximum [23], does not disperse laterally over a large propagation distance. In practice, like the idealized plane wave, no wave is forever diffraction-free due to finite energy considerations. Nonetheless, Bessel beams with useful large depths of field can be created. In addition to this propagation-invariant property, these Bessel beams can also reform after scattering from an object, the so-called "self-healing" property.

In analogy with light optics [22,24], electron Bessel beams were recently created from narrow annular apertures, and the self-healing property was demonstrated by scattering from an opaque wire [12], but the efficiency was expectedly low. More efficient electron Bessel beams have been produced using fascinating curved diffraction gratings to function as novel TEM apertures [11,25]. However, as with the annular aperture, this requires nanofabrication techniques to synthesize.

In early experimental work in light optics, McLeod [24] introduced the concept of the axicon lens, defined to focus an on-axis point source to a distribution of points behind the lens. Of the many possible types, which include the (conceptually simple) narrow annular aperture, the most effective is an optical element shaped as a cone. In scalar wave optics, it can be shown that a conical lens indeed focuses an incident plane wave to a Bessel beam in the near field of the axicon [26], provided that the cone imparts a strictly linear phase ramp in the transverse radial direction [Fig. 1(a)] (compared with a conventional convex lens that introduces a quadratic phase shift in that direction).

For the case of electrons, an efficient axicon lens has yet to be reported in electron microscopy, to the best of our knowledge. In this Letter, we demonstrate a natural method to synthesize a linear electron phase ramp along the radial direction from the core of a magnetic vortex structure to provide an electron axicon lens. We show experimentally that this electron axicon lens is an efficient and practical means to generate an electron Bessel beam in a TEM. First let us consider how to generate a linear phase ramp for electrons, which acts as an axicon lens. When electrons are transmitted through a thin film, the electron phase will be

modulated by the material's inner electrostatic potential V_0 and magnetic field B_n (for magnetic samples), as follows [27–29]:

$$\phi(r) = C_E \int_{-\infty}^{+\infty} V_0(r,z)dz - \frac{e}{\hbar}\int_{-\infty}^{+\infty}\int_{r}^{+\infty} B_n(\rho,z)d\rho dz, \qquad (1)$$

in cylindrical coordinates (omitting the chosen fixed polar angle), where r is the radial distance along a direction in the plane of the sample, z is the distance along the incident electron beam direction, e is the electron charge, $\hbar$ is the reduced Planck constant, C_E is the "interaction constant," which varies with the electron wavelength [30], and $B_n(r,z)$ is the component of the magnetic induction perpendicular to r direction. The phase shift due to $B_n(r,z)$ is often also written in terms of the z component of the magnetic vector potential using Stokes' theorem [31,32]. From this equation, it is evident that one approach for generating an electron axicon lens would be to engineer variations in the inner electrostatic potential, either via compositional variations in a planar specimen or by sculpting the three-dimensional (3D) shape of a homogenous material. We have demonstrated previously that a semiconductor (Si,Ge) alloy island with a truncated pyramidal shape can introduce such a linear phase ramp on incoming electrons [33]. Similar electrostatic phase plate approaches have also been applied for electron vortex beams [34]. However, the electron phase shift introduced by a material's mean inner potential is small, so that a thick film has to be used to introduce a sufficient phase shift to act as an axicon lens. For example, to generate a 20π phase shift for 200 keV incident electrons ($C_E = 0.007\,29\ \mathrm{V^{-1}\,nm^{-1}}$), a wedged Si crystal (mean inner potential 12.57 V [35]) with a maximal thickness of ~700 nm is needed. This is impractically thick; the electron amplitude will be seriously damped due to inelastic scattering. Furthermore, wrapping the phase shift into 2π by periodic modulation of the film thickness is very challenging for nanofabrication.

It is also evident from Eq. (1) that the magnetic field shifts the electron phase but in a different way. Electrons are deflected orthogonal to the moment distribution in proportion to the magnetization. Even for a constant thickness of magnetic thin film, the electrons will achieve a continuous linearly varying phase shift under the effect of the Lorentz force. This can generate a sufficient in-plane phase shift without the need to change the specimen thickness. Micromagnetic simulations coupled with magnetic force microscopy [36] and off-axis [32,37,38] and phase contrast [39] electron holography have shown that magnetic moments point out of plane in a small neighborhood of the magnetic vortex origin, with interesting applications for four state logic elements afforded by this additional magnetic substructure [39]. For an electron axicon comprising a strictly in-plane magnetic vortex, such small orthogonal magnetic moments aligned with the optic axis contribute no phase shift in projection and therefore do not affect the axial focusing of the electrons.

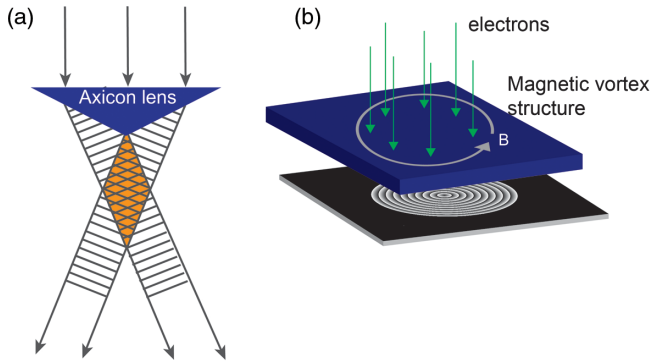

FIG. 1. (a) Cross section of a conical axicon lens inducing a rotationally linear phase ramp which superposes plane waves in a focal volume where the nondiffracting Bessel beam is formed. In the far field, an annular beam profile is created. (b) Electrons incident upon an orthogonal thin film containing a magnetic vortex suffer a conical phase shift identical to that created by an axicon lens.

Beleggia and Zhu [40] have derived the magnetic linear phase shift ϕ, imparted on a fast electron plane wave by a circularly magnetized disk of constant film thickness t:

$$\phi(r) = -\frac{e}{\hbar} B_n\, t r, \qquad (2)$$

where r is the transverse radial distance from the magnetic vortex center (here we have offset the phase to be zero at the core). Thus, a magnetic vortex in a thin film or a single particle with uniform thickness will induce a linear conical phase shift in a TEM [Fig. 1(b)], directly analogous to a conical optical element for generating an optical Bessel beam [Fig. 1(a)].

Here we demonstrate experimentally the efficient creation of Bessel beams from electron axicons, using the remarkable focusing ability of naturally occurring magnetic vortices. These topological moment configurations are ubiquitous in soft-magnetic films and isolated magnetic particles, as the flux-closure state is energetically favored for particles above a certain size [41].

Nanocrystalline FeCo-based soft-magnetic alloys were synthesized by melt spinning and subsequent annealing [42]. An alloy ribbon was thinned to electron transparency using ion milling. Phase contrast imaging and electron holography experiments were performed using a JEOL 2200FS field emission gun TEM operating at 200 kV. The main objective lens of the TEM was turned off to ensure a magnetic-field-free environment to observe magnetic domain structures, which defines the Lorentz mode. An objective minilens below the lower pole piece was used for phase contrast through-focus imaging to obtain Lorentz images. An electron biprism located near the first image plane was used to measure the interference between

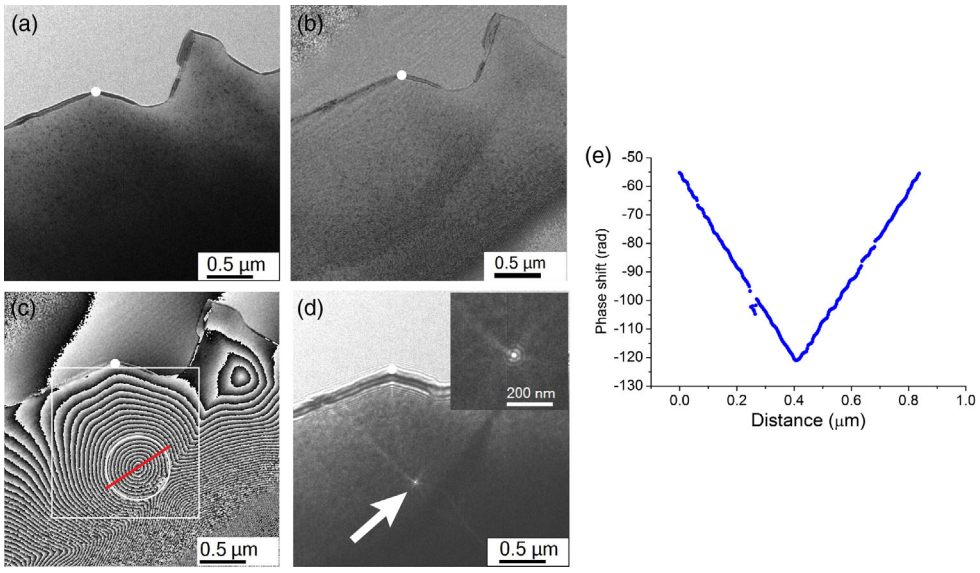

FIG. 2. (a) Near focus Lorentz image of a FeCo-based soft magnet thin film. (b) Electron wave amplitude reconstructed from the off-axis hologram. (c) Phase of the electron wave at the specimen plane, showing a conical linear ramp created by a magnetic vortex, consistent with an electron axicon lens. (d) Defocused Lorentz image portraying a locally focused probe with a Bessel-like ring structure, perturbed by domain walls and specimen boundaries. (e) Linear phase ramp measured along the inset red line in (c), after unwrapping the modulo-2π discontinuities.

electron waves passing through the specimen and reference waves propagating in the vacuum, near the edge of the specimen, as recorded in off-axis electron holograms using a Gatan slowscan 794 CCD camera. The electron biprism voltage was 70 V, and the vacuum fringe spacing was 11.9 nm. The electron holograms were Fourier processed [43], to retrieve the phase and amplitude of the electron wave exiting the magnetic thin film.

To examine the focusing behavior of this localized magnetic vortex, the biprism was retracted and a through-focus series of Lorentz images was acquired. In addition, using the reconstructed electron exit wave function, a focal series of synthetic phase contrast images was created to implement Fresnel propagation.

The specimen region of interest is shown in Fig. 2, containing an in-focus Lorentz image and electron hologram reconstructions. The electron intensity image in Fig. 2(a) shows only the structure contrast, where sparse nanocrystals cause the mottled contrast amid the amorphous matrix. Figure 2(b) is the amplitude image reconstructed from the hologram, which has similar contrast to Fig. 2(a). In Fig. 2(c), the reconstructed phase image, large contour lines with phase spacing 2π clearly indicate the in-plane magnetic flux density B_0 in the thin film. The phase image shows a large magnetic vortex structure in the center of the image. A phase line profile (after the phase is unwrapped) through the center of the vortex is plotted in Fig. 2(e). It shows a linear phase ramp of the vortex structure, consistent with an axicon lens. Note that the sign of the shift in Fig. 2(e) differs from Eq. (2) (for positive B_n), due to the alternate circulation of the in-plane magnetic field, and we have alternatively chosen the unwrapped phase to be zero in the vacuum. The electron axicon focus can be real [as in Fig. 2(d)] or virtual, depending upon the chirality of the magnetic vortex, which can be changed by flipping the sample over. The phase gradient is measured to be 162 rad/μm. The magnetic flux density B_0 has been measured from a bulk sample as 1.3 T. According to Eq. (2), the film thickness in the vortex region is then estimated to ~82 nm.

To examine the effect of this magnetic vortex, Fig. 2(d) shows a defocused Lorentz image of the electron intensity distribution below the sample with a nominated electron propagation distance of 1536 μm. As highlighted by the arrow, a focused electron beam is formed there. The multiple rings around the bright center clearly show the typical character of a Bessel beam (see the inset). It proves that the magnetic vortex acts as an electron axicon and deflects the electrons into a cone structure (despite the interfering contributions from the nonuniform specimen morphology and contrasting magnetic structure adjacent to the circularly symmetric magnetic vortex). These observations are consistent with Fig. 2(c), since, far from the magnetic vortex core, the wrapped contours indicate lines of strong phase curvature. These radial lines act as cylindrical focusing elements which, upon wave propagation, cause the observed streaks.

To further verify the formation of the Bessel beam, the electron intensity at different distances from the axicon lens was recorded by a focal series of Lorentz microscopy images, as shown in Fig. 3. The contrast in the resulting experimental images [Fig. 3(a)] is in agreement with the simulated electron intensity distribution [Fig. 3(b)] and

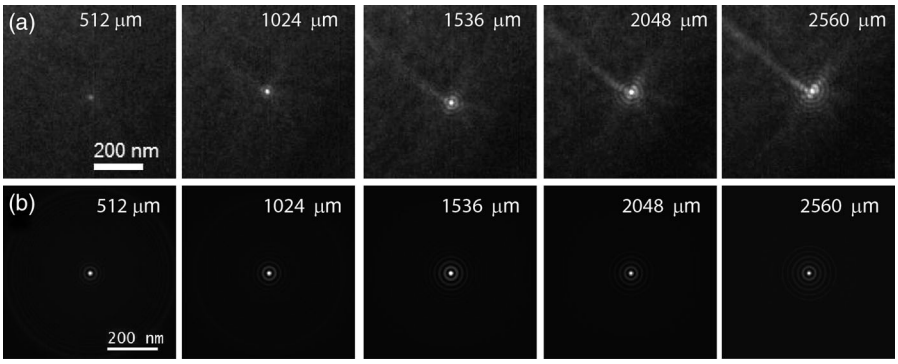

FIG. 3. (a) Experimental through-focus series from the specimen region inset in Fig. 2(d), showing the preservation of the beam profile and central waist over a nominal 2.56 mm focal range. (b) Simulated through-focus series for a perfect axicon, using the linear phase gradient inferred from Fig. 2(c).

clearly shows the nondiffracting nature of the electron Bessel beam. In the corresponding simulation, a plane wave was transmitted through an ideal circular vortex phase plate with the phase gradient 162 rad/μm and propagated to the nominated distance.

Since the complete electron wave front (amplitude and phase) at the exit plane of the magnetic axicon lens was recorded by electron holography (Fig. 2), it was possible to calculate the electron distribution at any distance from the axicon lens by considering Fresnel propagation of the wave in a vacuum, without the need for physical imaging. This provided the unique possibility to explore further the diffracting-free nature of the generated electron Bessel beam. The electron intensity distribution at each plane up to 5 mm from the magnetic axicon lens was hence calculated and plotted as a cross-section view in Fig. 4.

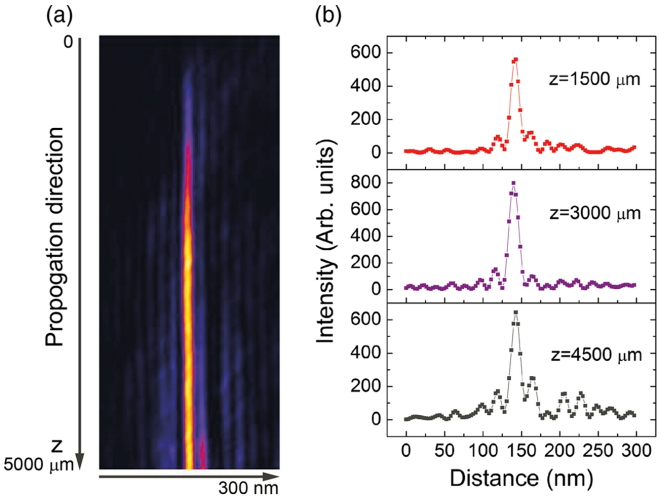

FIG. 4. Continuous focal series propagated from the off-axis hologram recorded electron wave, using a virtual square aperture outlined in Fig. 2(c), showing the diffraction-free property of the electron beam focused by a magnetic vortex. (a) Cross-sectional intensity profile as a function of the propagation distance. (b) Transverse intensity profiles at 1500, 3000, and 4500 μm.

The transverse intensity line profile at propagation distances of 1500, 3000, and 4500 μm was taken from the calculated 3D electron intensity and plotted in Fig. 4(b). Figure 4 clearly shows that the central lobe does not spread, even after very long propagation distances.

Importantly, the electron axicon lens can also generate an electron donut beam in the transmission electron microscope. The linear phase ramp tilts the beam into a cone structure, so that the electrons will form a ring structure in the far field diffraction plane. To demonstrate this experimentally, we used a virtual selected-area aperture to select the central, unperturbed part of the vortex, since the complete wave front (amplitude and phase) was recorded in the electron hologram. A resultant ring structure for the electron beam was obtained ("donut beam") [Fig. 5(a)], in agreement with the simulation using a perfect axicon lens [Fig. 5(b)]. Electron Bessel beams have potential applications as electron tweezers to move nanoparticles in a TEM [44–46].

The intrinsic efficiency of this electron axicon lens is remarkable. Although the experimental results shown in Figs. 2–5 are from an imperfect axicon lens. As evident in Fig. 2, the magnetic vortex of interest was in close proximity to the specimen edge and other magnetic domains, so the

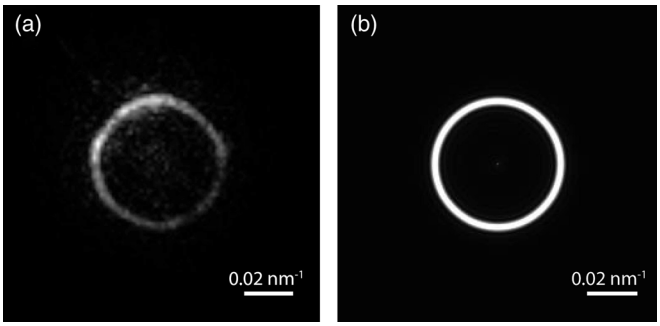

FIG. 5. (a) Fraunhofer diffraction pattern from the generated electron Bessel beam wave function using the circular aperture outlined in Fig. 2(c), compared to (b) the simulated result, showing the ring structure characteristic of a Bessel beam.

shape anisotropy slightly perturbed the circular domain structure, causing the radial flares of Fresnel fringes emanating from the Bessel beam core in the Lorentz image of Fig. 2(d). Nonetheless, the characteristic Bessel beam profile and its nondiffracting focal evolution were still observed in our quantitative measurements. This is a testament to the robustness in the presence of perturbations, likely a consequence of the intrinsic self-healing property of the Bessel beam. Judging from our analytic simulations, specifically designed disk-shaped magnetic nanoparticles are expected to produce higher-quality electron Bessel beams with even larger millimeter-scale depths of focus. Conventional methods for producing electron Bessel beams, such as narrow annular apertures or binary curved gratings, necessarily partly block the beam—in the case of a thin annulus, an ideal annular aperture should block almost all of the incident wave to ensure nondiffracting conditions. Intrinsic to the efficiency of the phase modulation approach described here is that it does not attenuate the beam. However, there will be inelastic scattering in the magnetic alloy which will reduce the monochromaticity of the beam. For the ~80 nm foil used here, approximately 50% of the electrons will have suffered an inelastic event (see Supplemental Material [47]). We also note that the magnetic vortex electron axicon does not require an additional lens to create the Bessel beam or the expanding donut beam, unlike aperture-based approaches.

In this Letter, the axicon lens was placed in the specimen plane, to prove the principle that a magnetic object can be used to craft the phase of electron waves, using a Bessel beam as a particular example. This demonstrates an entirely different approach to controlling electron wave fields in electron-optical systems, such as transmission and scanning electron microscopes. From a practical perspective, magnetic vortices of this type, whether naturally occurring or engineered, are on the scale of microns or larger and can readily be inserted in conventional electron microscope aperture mechanisms and in different electron-optical planes. Indeed, other suitable linear phase ramps for electron waves imparted by magnetic flux closure domains can readily be fabricated [36,48] and have been clearly demonstrated in electron holography [49,50]. Furthermore, the alloy is highly conductive, robust under electron irradiation, and illuminated with a relatively low current density, planar wave field. It is therefore expected to have a long lifetime under practical operating conditions. Stemming from the present work, other forms of magnetic phase modulators can be envisaged.

In the present work, we have demonstrated the use of a magnetic vortex as a linear phase modulator to act as an electron axicon lens. Several other applications of such magnetic phase modulators can be envisaged. For example, as indicated in Eq. (1), a higher-order phase shift could also be achieved by engineering the sample thickness in the magnetic vortex. As another example, a lattice of Bessel beams could be generated from an array of magnetic vortex domains [49], with interesting potential applications, such as a Hartmann-like sensor [51] for electron wave front sensing.

Here we have considered elementary magnetic moment distributions to sculpt a nondiffracting electron probe. Singular electron optics aside, this work further espouses the merits of magnetic moment configurations for designing electron phase plates in conjunction with electrostatic refraction [7,15,52,53].

We have shown that electron Bessel beams can be created efficiently by using magnetic vortices as electron axicon lenses. Such electron axicons naturally occur in soft-magnetic alloys, as well as circular magnetic particles containing energetically preferred flux-closure magnetization distributions. The electron axicon and Bessel beam confirmed in this work present opportunities for fabricating similarly efficient isolated conical phase plates from magnetic disks. Coupled with millimeter depths of focus, such electron axicons could enable new probe forming and/or wave front sensing capabilities in electron microscopy. More generally, this work further illustrates the potential for engineering magnetic vortex structures to generate tailored phase plates, providing a highly efficient and flexible way to shape an electron wave field to probe matter in new and targeted ways.

We thank Dr. J. Long, Professor D. Laughlin, and Professor M. McHenry (Carnegie Mellon University) for providing the FeCo-based alloy sample. We also thank Professor David Paganin (Monash University) for many helpful suggestions. This work was supported in part by funding from the Australian Research Council Discovery Project Grant No. DP160104679.

*Corresponding author.
joanne.etheridge@monash.edu

[1] K. Y. Bliokh, Y. P. Bliokh, S. Savel'ev, and F. Nori, Phys. Rev. Lett. **99**, 190404 (2007).
[2] M. Uchida and A. Tonomura, Nature (London) **464**, 737 (2010).
[3] J. Verbeeck, H. Tian, and P. Schattschneider, Nature (London) **467**, 301 (2010).
[4] B. J. McMorran, A. Agrawal, I. M. Anderson, A. A. Herzing, H. J. Lezec, J. J. McClelland, and J. Unguris, Science **331**, 192 (2011).
[5] L. Clark, A. Beche, G. Guzzinati, A. Lubk, M. Mazilu, R. Van Boxem, and J. Verbeeck, Phys. Rev. Lett. **111**, 064801 (2013).
[6] T. C. Petersen, M. Weyland, D. M. Paganin, T. P. Simula, S. A. Eastwood, and M. J. Morgan, Phys. Rev. Lett. **110**, 033901 (2013).
[7] A. Beche, R. Van Boxem, G. Van Tendeloo, and J. Verbeeck, Nat. Phys. **10**, 26 (2014).
[8] A. Beche, R. Juchtmans, and J. Verbeeck, Ultramicroscopy (to be published).
[9] N. Voloch-Bloch, Y. Lereah, Y. Lilach, A. Gover, and A. Arie, Nature (London) **494**, 331 (2013).

[10] G. Guzzinati, L. Clark, A. Beche, R. Juchtmans, R. Van Boxem, M. Mazilu, and J. Verbeeck, Ultramicroscopy **151**, 85 (2015).
[11] V. Grillo, E. Karimi, G. C. Gazzadi, S. Frabboni, M. R. Dennis, and R. W. Boyd, Phys. Rev. X **4**, 011013 (2014).
[12] K. Saitoh, K. Hirakawa, H. Nambu, N. Tanaka, and M. Uchida, J. Phys. Soc. Jpn. **85**, 043501 (2016).
[13] T. C. Petersen, D. M. Paganin, M. Weyland, T. P. Simula, S. A. Eastwood, and M. J. Morgan, Phys. Rev. A **89**, 063801 (2014).
[14] J. Verbeeck, H. Tian, and G. Van Tendeloo, Adv. Mater. **25**, 1114 (2013).
[15] G. Guzzinati, A. Béché, H. Lourenço-Martins, J. Martin, M. Kociak, and J. Verbeeck, Nat. Commun. **8**, 14999 (2017).
[16] P. Schattschneider, T. Schachinger, M. Stoger-Pollach, S. Loffler, A. Steiger-Thirsfeld, K. Y. Bliokh, and F. Nori, Nat. Commun. **5**, 5586 (2014).
[17] R. Juchtmans, A. Beche, A. Abakumov, M. Batuk, and J. Verbeeck, Phys. Rev. B **91**, 094112 (2015).
[18] M. Stöger-Pollach, T. Schachinger, K. Biedermann, and V. Beyer, Ultramicroscopy **173**, 24 (2017).
[19] P. Schattschneider, V. Grillo, and D. Aubry, Ultramicroscopy **176**, 188 (2017).
[20] D. Nguyen, J. Etheridge, and S. Findlay (to be published).
[21] W. D. Montgomery, J. Opt. Soc. Am. **58**, 1112 (1968).
[22] J. Durnin, J. J. Miceli, and J. H. Eberly, Phys. Rev. Lett. **58**, 1499 (1987).
[23] J. Durnin, J. J. Miceli, and J. H. Eberly, Phys. Rev. Lett. **66**, 838 (1991).
[24] J. H. McLeod, J. Opt. Soc. Am. **44**, 592 (1954).
[25] V. Grillo, J. Harris, G. C. Gazzadi, R. Balboni, E. Mafakheri, M. R. Dennis, S. Frabboni, R. W. Boyd, and E. Karimi, Ultramicroscopy **166**, 48 (2016).
[26] J. Jahns and S. Helfert, *Introduction to Micro-and Nanooptics* (Wiley, New York, 2012).
[27] A. Tonomura, *Electron Holography* (Springer, Berlin, 1999).
[28] H. Lichte and M. Lehmann, Rep. Prog. Phys. **71**, 016102 (2008).
[29] M. R. McCartney and D. J. Smith, Annu. Rev. Mater. Res. **37**, 729 (2007).
[30] J. M. Cowley and A. F. Moodie, Acta Crystallogr. **10**, 609 (1957).
[31] Y. Aharonov and D. Bohm, Phys. Rev. **115**, 485 (1959).
[32] M. Beleggia, M. A. Schofield, Y. Zhu, M. Malac, Z. Liu, and M. Freeman, Appl. Phys. Lett. **83**, 1435 (2003).
[33] C. L. Zheng, K. Scheerschmidt, H. Kirmse, I. Hausler, and W. Neumann, Ultramicroscopy **124**, 108 (2013).
[34] R. Shiloh, Y. Lereah, Y. Lilach, and A. Arie, Ultramicroscopy **144**, 26 (2014).
[35] P. Kruse, M. Schowalter, D. Lamoen, A. Rosenauer, and D. Gerthsen, Ultramicroscopy **106**, 105 (2006).
[36] T. Shinjo, T. Okuno, R. Hassdorf, K. Shigeto, and T. Ono, Science **289**, 930 (2000).
[37] A. Tonomura, T. Matsuda, J. Endo, T. Arii, and K. Mihama, Phys. Rev. Lett. **44**, 1430 (1980).
[38] W. X. Xia, S. Aizawa, T. Tanigaki, T. Suzuki, Y. Yoshizawa, D. Shindo, and A. Tonomura, J. Electron Microsc. **61**, 71 (2012).
[39] C. Phatak, M. Tanase, A. K. Petford-Long, and M. De Graef, Ultramicroscopy **109**, 264 (2009).
[40] M. Beleggia and Y. Zhu, Philos. Mag. **83**, 1045 (2003).
[41] R. P. Cowburn, D. K. Koltsov, A. O. Adeyeye, M. E. Welland, and D. M. Tricker, Phys. Rev. Lett. **83**, 1042 (1999).
[42] J. G. Long, P. R. Ohodnicki, D. E. Laughlin, M. E. McHenry, T. Ohkubo, and K. Hono, J. Appl. Phys. **101**, 09N114 (2007).
[43] M. Takeda, H. Ina, and S. Kobayashi, J. Opt. Soc. Am. **72**, 156 (1982).
[44] V. P. Oleshko and J. M. Howe, Ultramicroscopy **111**, 1599 (2011).
[45] D. W. Zhang and X. C. Yuan, Opt. Lett. **28**, 740 (2003).
[46] A. A. Gorlach, M. A. Gorlach, A. V. Lavrinenko, and A. Novitsky, Phys. Rev. Lett. **118**, 180401 (2017).
[47] See Supplemental Material at http://link.aps.org/supplemental/10.1103/PhysRevLett.119.174801 for Electron energy loss spectroscopy to measure inelastic scattering proportion and estimate the electron axicon efficiency.
[48] T. Okuno, K. Shigeto, T. Ono, K. Mibu, and T. Shinjo, J. Magn. Magn. Mater. **240**, 1 (2002).
[49] Y. Zhu, V. V. Volkov, M. Schofield, M. Beleggia, J. Lau, and M. Malac, Microsc. Microanal. **9**, 442 (2003).
[50] S. Bajt, A. Barty, K. A. Nugent, M. McCartney, M. Wall, and D. Paganin, Ultramicroscopy **83**, 67 (2000).
[51] R. V. Shack and B. C. Platt, J. Opt. Soc. Am. **61**, 648 (1971).
[52] R. M. Glaeser, Rev. Sci. Instrum. **84**, 111101 (2013).
[53] K. Nagayama, Eur. Biophys. J. **37**, 345 (2008).